**Title**
Orientation-dependent handedness of chiral plasmons



**Author**
Rodriguez, Kate

**Publication Date**
2018

Peer reviewed|Thesis/dissertation

UNIVERSITY OF CALIFORNIA,
IRVINE

# Orientation-dependent handedness of chiral plasmons

THESIS

submitted in partial satisfaction of the requirements
for the degree of

MASTER OF SCIENCE

in Chemical and Materials Physics

by

Kate Rodriguez

Thesis Committee:
Professor V. Ara Apkarian, Chair
Professor Matt Law
Professor Eric Potma

2018

# DEDICATION

To

my family and friends

in recognition of their continued support.

On the unexpected:

“The most beautiful thing we can experience

is the mysterious.

It is the source of all true

art and science.”

Albert Einstein
*Living Philosophies*

# TABLE OF CONTENTS

# LIST OF FIGURES

# LIST OF TABLES

# ACKNOWLEDGMENTS

I would like to thank my committee chair and advisor, Ara Apkarian, for his support and encouragement during the progression of this project. The orientation-dependent handedness this thesis will elaborate on certainly was an unexpected effect. His open-door policy, and continued willingness to thoroughly discuss all aspects of the science with his students, was paramount to the project's success.

I would also like to thank my committee members, Professor Matt Law and Professor Eric Potma, for their support and willingness to serve as committee members.

Finally, I would like to thank my undergraduate research advisors, Professor Robbie J. Iuliucci, Professor William Sheers, and Professor Rosalynn Quiñones, for encouraging me to pursue science all those years ago.

Financial support was provided by the NSF Center for Chemical Innovation, Chemistry at the Space-Time Limit (CaSTL) under grant CHE-1414466.

# ABSTRACT OF THE THESIS

Orientation-dependent handedness of chiral plasmons

By

Kate Rodriguez

Master of Science in Chemistry

University of California, Irvine, 2018

Professor V. Ara Apkarian, Chair

Optical activity has long been an area of interest in Raman scattering spectroscopy as it is a powerful tool for elucidating molecular chirality. Here, I provide details from an investigation into plasmonic (rather than molecular) optical activity in surface-enhanced Raman spectroscopy. The sample used is the prototypical dumbbell nano-antenna (nantenna) consisting of two gold nanospheres functionalized with bipyridyl ethylene molecular reporters. Previous analysis of the linear dichroism reveal that the structures scatter as dipolar antennas, with the molecular vibrations following the polarization patterns of the dumbbell on which they reside. Current investigations into circular optical activity of the nantenna reveal two notable observations. First, the Raman optical activity is at least two orders of magnitude larger than values typically observed for molecular species. Second, the observed handedness of the dumbbell is entirely dependent on its orientation in the plane perpendicular to excitation.

We attribute this counter-intuitive effect to the multipolar response of the plasmonic nantenna, which arises from its large size with respect to the excitation wavelength ($\sim\lambda/2$). Here, the long-wave approximation breaks down and retardation

effects can no longer be ignored, giving rise to the inclusion of the electric quadrupole and magnetic dipole modes in addition to the zeroth-order electric dipole. The observed ODH can be understood in terms of the electric and magnetic dipole terms, which appear to undergo a simultaneous time reversal operation upon in-plane rotation. These results are explained in the framework of Jones calculus and have important implications in the treatment of bi-isotropic media.

# 1. INTRODUCTION

## 1.1. Surface enhanced Raman on plasmonic nantennas

In the historic push toward single molecule detection, surface enhanced Raman spectroscopy (SERS) has emerged as a powerful and multifaceted technique due to its high enhacement factors (>$10^8$ in some cases) (1) and broad range of applicability to various samples (2). Although there are several ways of engineering SERS-capable systems, of particular interest is the so-called “dumbbell” dimer nano-antenna (nantenna), consisting of two metallic nanospheres functionalized with a molecular reporter (3). The nantenna nomenclature is a nod to the classical Hertzian dipole antenna to which the dumbbell serves as a nano-scale analog (4). Here, the metallic nanospheres confine incident radiation to the nm-scale inter-sphere junction; this high degree of spatial confinement of the fields contributes to the dramatic enhancement factors observed in these structures (3).

The particular geometry utilized here is two gold nanospheres, ~100 nm in diameter each, linked with bipyridyl ethylene (BPE) molecular reporters. This puts the total size of the dimer at nearly 200 nm, or approximately $\lambda/2$ for optical excitation wavelengths. At this size, the dipolar approximation fails – the dimer is large enough to experience field gradient effects and, as such, spatial dispersion must be taken into account. Doing so culminates in the inclusion of both magnetic dipole and electric quadrupole terms, in addition to the zeroth order (long-wavelength limit) electric dipole (5). Experimentally, the inclusion of these higher order multipoles is verified by polarization-resolved Raman scattering measurements – we find that all three terms are required to correctly reproduce the observed sample scattered intensity patterns. These

experiments (and their subsequent fits) will be discussed in more detail accordingly; here, we focus instead on the qualitative consequences that arise from plasmonic multipolar Raman.

One immediate consequence of multipolar response is an additional enhancement: in general, the ratio of magnetic to electric dipolar transitions scale as $|\vec{m}|^2/|\vec{d}|^2 \sim |\vec{k}\cdot\vec{r}|^2 = |2\pi\vec{r}/\lambda|^2$ (5). This ratio is approximately unity for a $\lambda/2$ antenna such as our dimer; compared to the ratio in the long-wavelength limit ($10^{-4}$), we gain an additional enhancement of $10^4$ beyond strictly dipolar Raman scattering. This provides the basic mechanism by which phenomena such as linear dichroism and optical activity in SERS are made possible. The two proceeding sections will elaborate on these observations in more detail.

## 1.2. Previous results: Linear dichroism

The first set of polarization-resolved SERS experiments put forth by the Apkarian lab were investigations into linear dichroism. A halfwave plate (HWP) was used to sweep out incident linear polarization through 360° with Raman spectra recorded every few degrees. The scattered signal is decomposed into two orthogonal channels, one parallel and one perpendicular to the incident linear polarization, to allow for full characterization of the material response. The details of this experiment are presented elsewhere (6); here we note only that, as shown in Fig. 1, the dimers scatter as typical dipolar antenna. Although all polar plots presented in this document are integrated over the 1640 $cm^{-1}$ molecular vibration of the reporter molecule (BPE), in all cases the

molecular reporter merely follows the dimer scattering pattern – *i.e.*, it is the antenna polarization alone that is broadcast to the far-field.

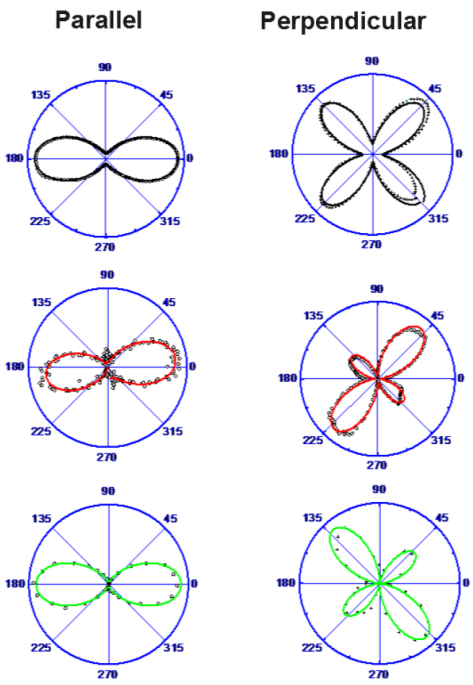


Figure 1.1: Linear optical activity. Results from three representative dimers under linear OA measurements. The first dimer is a symmetric dipolar antenna, while the following two display scattering asymmetry in the perpendicular channel. This asymmetry was the first evidence of OA exhibited by the dimers, and was the inspiration for the circular OA experiments that will be the focus of this thesis.

Though the parallel channel shows symmetric dipolar response in all cases, unique asymmetry is sometimes observed in the perpendicular channel when the incident excitation is polarized along $\pm 45°$ with respect to the antenna long (interparticle) axis. This is an interesting realization of plasmonic linear dichroism which lead us to believe that the dimers exhibit some inherent handedness, here with respect to $\pm 45°$ light. The most natural extension of this experiment is to then use circularly polarized light (CPL) to investigate the chiral nature of these plasmonic nanoparticles.

## 1.3. Chirality, handedness, and optical activity

Before we proceed further, it is useful to define the terms *chirality* and *handedness* both in general and as applied to plasmonic systems. The definition of *chiral* in the framework of optical activity (OA) refers to an object that is not superimposable onto its mirror image. For some chiral objects, such as a shoe, the *handedness* is immediately apparent – you can, for example, immediately tell if a shoe belongs on your left or right foot. For more complicated structures, such as molecules whose handedness is not immediately apparent, we instead must inspect their interactions with CPL (either right- or left-handed) as an object will interact preferentially with light of its same handedness (7).

Traditionally, OA in Raman spectroscopy refers to studies of chiral molecules under right- (RCP) and left-handed (LCP) CPL. We distinguish this from our resulting OA experiments, as the chirality here arises from the optical response of the nantenna and is therefore plasmonic, rather than molecular, in nature. Nevertheless, the treatment of OA is equivalent in either case. The extent of OA is calculated by taking the difference in scattered intensity between SERS spectra collected under RCP and LCP, which is typically very weak (on the order of ppt) for molecular species (8). In terms of molecular OA, the phenomenon is attributed to the compound action of the polarizability and optical activity tensors, whereby scattered light contains explicit dependence on the degree of circular polarization of the excitation (9).

The definition of chirality in terms of non-superimposable mirror images, since based on a discrete transformation (reflection), leads to difficulty when attempts are made to quantify the extent of chirality. This ultimately culminates in the issue of chiral

connectedness: based on the historical definition of chirality, quantification efforts indicate that a mirror symmetric object should have chirality of zero, while the two enantiomers of a chiral object should be of opposite sign so that the sign of one enantiomer exactly inverts upon reflection into the other. In reality, however, any continuous object may be taken continuously from one enantiomer to the other such that *it reaches a state of zero chirality that is necessarily non-mirror symmetric*. Additionally, some mirror-symmetric objects are able to exhibit clear handedness, for example, due to extrinsic chirality generated by the relative orientations of the intrinsically achiral structure and the excitation source (10). Such considerations constitute the paradox of chiral connectedness and for many years hampered efforts into the quantification of chirality.

A more rigorous mathematical definition for quantifying chirality and handedness was given by Efrati and Irvine (11). In this work, the authors construct an object whose handedness depends entirely on the direction from which the object is viewed. In this way, the object can be made either RH or LH depending on how it is oriented in the plane parallel to excitation. By incorporating this orientation-dependence into the object's handedness tensor, chiral connectedness is now fully accounted for: this treatment allows for the explanation of objects that both lack mirror symmetry/have no net chirality and have mirror symmetry/have net chirality. It is with these characterizations in mind that we now proceed to our own ODH experiments.

## 1.4. Optical activity in plasmonic nantennas

The considerations undertaken in the series of experiments presented here differ from those of standard ROA and from previous orientation-dependent handedness for two critical reasons. First, as already mentioned, the chirality of the dimers arises from the multipolar Raman response of the plasmon, not of the molecular reporter – *i.e*., the chirality arises from the motion of the electrons comprising the plasmon. Though this initially seems far-removed from the structurally-derived handedness observed in many molecules, it is the very structure of the nantenna that, to large extent, dictates its plasmonic and scattering response. Second, the nantenna ODH is exhibited in the plane *perpendicular* to the excitation, rather than a plane parallel to it.

Effectively, as a result of these we will see that the OA of a typical dimer is (1) several orders of magnitude larger than is typically seen, and (2) forced to undergo a change in handedness under 90° in-plane rotation. Furthermore, the dimers embody chiral connectedness insofar as their handedness can be continuously varied from RH → achiral → LH meanwhile, even at their achiral orientation, they are still wholly chiral objects. This is analogous to a liquid cell filled with both RH and LH molecular enantiomers – the concentration can be varied continuously so that a predominantly RH mixture is eventually made racemic; though the racemic solution is not handed overall, it still cannot be superimposed onto its mirror image and thereby remains chiral.

The distinct nature of plasmonic chirality requires brief further comment here as it is, at its core, *chirality of motion*. As we will see in Chapter 4, the dimers sustain three dominant multipolar modes under visible light excitation: namely, the electric dipole, electric quadrupole, and magnetic dipole terms are simultaneously excited. The electric

and magnetic dipole terms are the crux of the plasmonic OA which is rationalized as follows. The electric dipole, which implies translation of charge, couples to the magnetic dipole, which drives charge circulation. The net effect of the two motions, translation + circulation, is helical motion – an inherently handed effect which naturally couples preferentially with light of the same handedness. This simple model serves as the basis for the entire plasmonic OA treatment.

Our goal is to describe a dimer in terms of its own 2D response function in **SU(2)**, it's so-called Jones matrix or, more formally, the familiar polarizability matrix of Raman. This matrix can be extracted directly from experimental data, working within the framework of Jones calculus. A more powerful treatment, however, comes from uniquely identifying the nature of each matrix element in terms of the direct multipolar modes – the generality of such a model allows for extensions to other systems and opens the door for a myriad of future applications.

# 2. EXPERIMENTAL

## 2.1. Sample preparation and initial characterization

All experiments are carried out on individual dimers, consisting of two gold spheres (100±10 nm in diameter each) laced with *trans*-1,2-bis(4-pyridyl)-ethylene (BPE) molecular reporters and coated with a silica shell (~70nm) for thermal stability. The sample, which is obtained in a water-based suspension from Cabot, is sonicated and subsequently dispersed onto a silicon nitride transmission electron microscopy (TEM) grid. At this point, the sample will contain several geometries – monomers, dimers, trimers, etc. The grid surface coverage is controlled via the concentration of the original solution dispensed onto the grid. We typically aim for relatively low coverage, with all particles separated from their nearest neighbors by at least a micron. Scanning electron microscopy (SEM) is used first to map out the surface of the TEM grid, allowing for identification of particle location and geometry.

## 2.2. Experimental geometry

SERS measurements are performed on a dual scan-probe/micro-Raman instrument (NT-MDT). The sample is mounted on an inverted optical microscope frame (Olympus, IX71) and illuminated with 532 nm CW laser excitation. The laser is focused using a variable 0.65-1.25 NA oil immersion objective lens. All scattered light is collected in the backwards direction with the Raman separated from the Rayleigh light via a pair of notch filters (Semrock, $1{:}10^6$ extinction ratio) and subsequently dispersed onto a 0.5 m monochromator and recorded by a CCD array (Andor, V401-BV). For sample mapping, the scan stage hosting the sample grid is raster scanned over the

stationary laser focus and the scattered light intensity is recorded pixel-by-pixel via a photodiode. This backscatter map, typically collected for a 50x50 μm range, is compared with the previously obtained SEM map in order to locate dimers of interest. As the laser spot size is ~1 μm diameter, dimers must be separated by 500 nm from all neighboring scatterers in order to be measured independently.

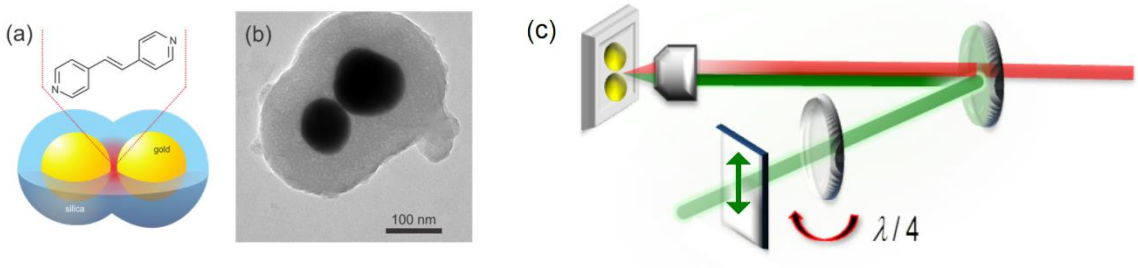


Figure 2.1: Sample and experimental setup. (a) Cartoon and (b) transmission electron micrograph of a typical dimer. (c) Experimental setup. 532 nm light is directed through a linear polarizer, followed by a quarter wave plate. A notch filter is used as a mirror to direct the polarization-controlled excitation toward the sample. After interaction, the red- and blue-shifted Raman signal passes through the notch filter and toward the detector.

## 2.3. Controlling polarization

To control polarization, two principle polarization optics are used: linear polarizer (LP) and quarter-wave plate (QW). The LP is oriented such that its fast axis is initially along the vertical (in the lab frame) for all measurements. The QW is placed directly after the LP and, depending on the orientation of its fast axis relative to the LP, generates the polarization states shown in Fig. 3a. When the QW fast axis makes an angle of $\chi = 0°, 90°, 180°, 270°$, w.r.t. the LP, vertically polarized light passes through unaltered. At $\chi = \pm 45°$, however, the QWP converts linearly polarized light into LH and

RH CPL, respectively, via the introduction of a 90° phase-shift between orthogonal polarization components. At intermediate angles, elliptical polarization is generated, with the handedness determined by the respective quadrant as shown below.

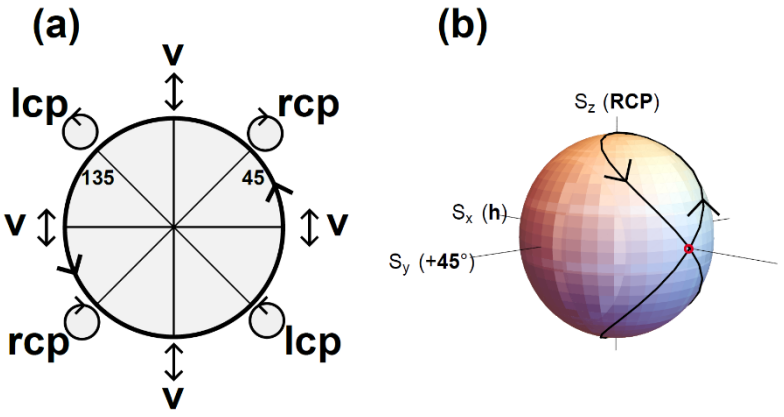


Figure 2.2: Polarization generated in the QW experiment. (a) Polarization generated as a function of the angle of the quarter wave plate fast axis relative to the vertical polarization incident upon it. (b) Corresponding path of the polarization states on the Poincare sphere. The light begins at vertical polarization and subsequently maps out a figure eight, moving upward in a counter clockwise fashion, on the surface of the sphere.

In many of our experiments, the QW is rotated continuously from $\chi = 0°$ to $\chi = 360°$, with spectra typically recorded every 5°. The resulting path of such an experiment is depicted on the Poincare sphere in Fig. 3b. The Poincare sphere is a unit sphere in which each point on the surface represents a distinct polarization state. The three orthogonal axes of the sphere are defined by the Pauli matrices $\{\sigma_1, \sigma_{2,}\sigma_3\} = \{\sigma_z, \sigma_{x,}\sigma_y\}$ of spin notation, with $\sigma_0$ defining the size of the sphere as unity. These axes correspond to $h/v$, $+45°/-45°$, $RCP/LCP$, respectively, and any polarization state is therefore determined by its projection into each axis (7). A point located at {-1, 0, 0}, for example,

would correspond to vertical polarization, while {0, 0, 1} corresponds to RCP. From this representation, we see continuously rotated the QW causes the polarization to evolve from vertical (red dot) → RCP (north pole) → vertical → LCP (south pole) as the QW is rotated through 180°; a 360° rotation simply retraces this figure-eight pattern once more. The results of subjecting various dimers to such continuous QW experiments are presented in the preceding chapter, at which time the full utility of the Poincare sphere will be realized.

# 3. RESULTS

## 3.1. Surface-enhanced Raman optical activity

A series of dimers were first analyzed under stationary RCP and LCP excitation to verify plasmonic OA; results for two representative cases are show below in Fig. 4. In both cases, the SERS signal of the dimers exhibit strong preference for either RH or LH CPL.

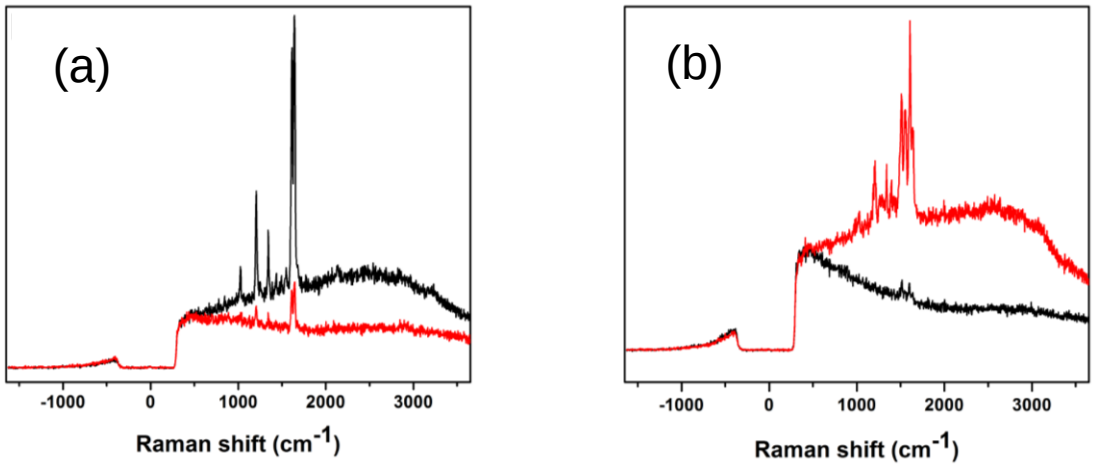


Figure 3.1: SERS OA on plasmonic nanodimers. Results of subjecting two dimers, (a) and (b), to LH (black) and RH (red) CPL. In both cases, the SERS spectra of the dimers show a clear preference to one CPL – LH in the case of (a), and RH in the case of (b). Note that the SERS spectra here consist of the discrete molecular vibrations atop a broad, continuous background that arises from the inelastic light scattering of the metal itself.

While ROA is normally a weak effect, the OA exhibited by the dimers is much more pronounced, on the order of parts per ten. Additionally, the effect is evident in both the molecular vibrational Raman lines (discrete peaks), as well as the metal electronic Raman scattering (continuous background). We define here the SERS circular OA as

$$OA = \frac{I_L - I_R}{I_L + I_R} \tag{3.1}$$

where $I_L$ and $I_R$ are the scattered intensity under LH and RH excitation, respectively. According to Eq. (1), positive values of *OA* indicate that the particle is left-handed, while negative values imply that it is right-handed. The resulting OA values for four example dimers are shown in Table 1.

| **Dimer** | **OA value** | **OA value** |
|---|---|---|
| | *Original* ($\varphi = 0°$) | *Rotated* ($\varphi = 90°$) |
| 1 | 0.73 | -0.15 |
| 2 | -0.31 | 0.2 |
| 3 | 0.8 | -0.23 |
| 4 | -0.86 | 0.2 |

Table 3.1: OA values for four selected dimers. Intensity here was integrated under the 1640 $cm^{-1}$ vibrational mode.

Here we noticed an interested trend – all of the dimers of a given handedness (*e.g.*, right-handed) were oriented similarly on the grid (*e.g.*, tilted towards the horizontal). To test if orientation had any effect on particle handedness, the entire sample substrate was subject to a 90° in-plane rotation. Remarkably, the measured values of *OA* exactly reverse in sign (though here, not in magnitude) for each particle analyzed (Table 1). This change in sign of the *OA* indicates a change in handedness of the dimers, indicating orientation-dependent handedness. The fact that the magnitudes are not fully recovered, however, is due to the random orientation of the particles, which will be elaborated on in great detail below.

These result highlight an interesting and counter-intuitive effect: namely, that particle handedness depends on its orientation in the plane perpendicular to excitation.

This effect has been observed in, to date, >50 dimers. Though most (>90%) show some degree of handedness, several remain entirely achiral regardless of their orientation. This we use in large part to argue that this is not an artifact (e.g., due to a tilt in the plane of the substrate). To rule out other sources of artifacts, we carry out the identical measurement on isotropic samples. We show in Fig. 5a that, as expected, identical Raman spectra are collected when liquid cyclohexane is excited by RCP and LCP light. We also not that the backscattered Rayleigh light on the dimers does not show the same degree of OA (Fig. 5b).

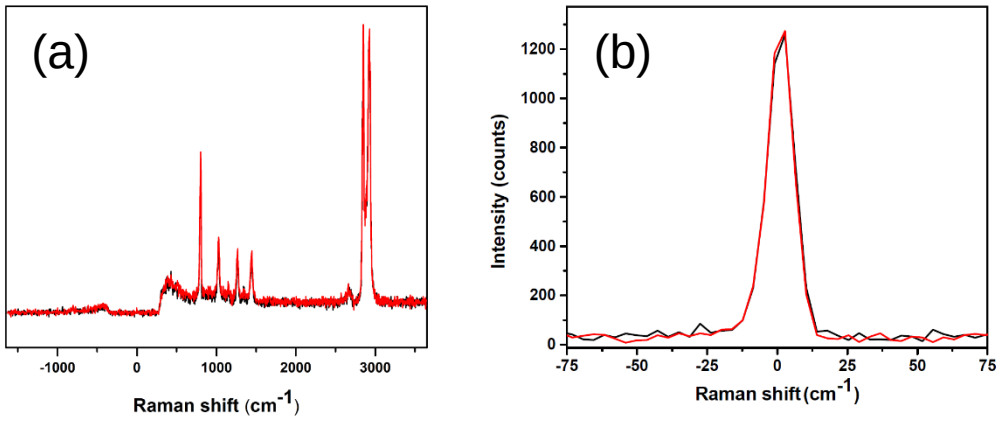


Figure 3.2: Control experiments. CPL controls, showing the contrast of LH vs RH excitation for (a) liquid cyclohexane and (b) the Rayleigh line of dimer 1 (Fig. 4a). In both cases, there is no measurable difference in response to LH and RH CPL.

## 3.2. Continuous polarization response

To further quantify the observed ODH, the Raman response of another dimer, dimer 5, was monitored continuously for a full 360° rotation of the QW, as discussed in Chapter 2. The polar plot of the SERS scattering intensity of dimer 5 as a function of the QW angle is shown in Fig. 6, at both is original (a) and rotated (b) positions. We will use

$\varphi$ to denote the orientation of the dimer within the substrate plane. Here, the original position corresponds to the dimer oriented horizontally ($\varphi = 0°$), *i.e.*, cross-polarized with the initial vertical polarization at QW orientation $\chi = 0°$, while it's rotated position puts it along the vertical ($\varphi = 90°$).

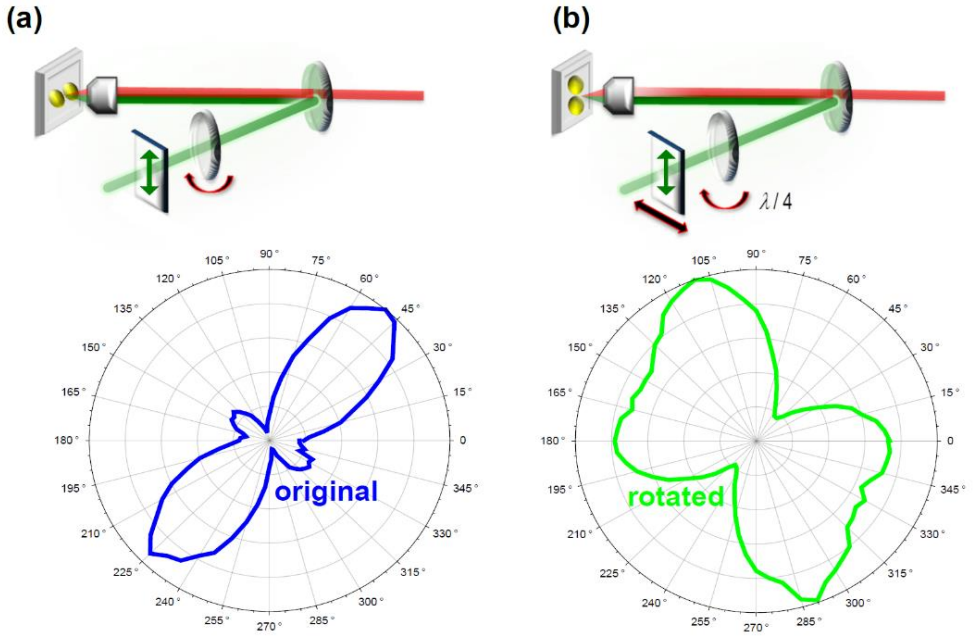


Figure 3.3: Results from QW rotation experiment, as performed on dimer 5. Plots trace the intensity of the 1640 cm$^{-1}$ vibrational line as a function of QW angle with respect to incident vertical polarization, $\chi$. Blue trace corresponds to the original position ($\varphi$~0°, with the dimer cross-polarized to the initial vertical light) and green to the rotated position ($\varphi$~90°, with the dimer aligned with the initial vertical light). Note here that the increased response around $\chi = 0°, 90°, 180°, 270°$ in the green plot is due to the dimer being aligned to the vertical polarization generated at these angles of the QW. Evidently, this particle underwent a change in handedness from RH → LH due to the in-plane rotation.

The ODH in dimer 5 is recognized by noting the change in its angle of maximum scattering intensity. At its original orientation it displays a clear preference for RCP, near $\chi = 45°$. Upon rotated, the dimer now appears to be largely LH, peaking near $\chi = 110°$.

Additionally, as this particle was orientated initially along $\hat{x}$ and, after rotation, along $\hat{y}$, its measured value of OA exactly inverts in both sign and magnitude ($OA_{\varphi=0^\circ} = 0.6, OA_{\varphi=90^\circ} = -0.6$).

# 4. ANALYSIS

## 4.1. Light-matter interaction

Given that an object is uniaxial and has dimensions on the order of the wavelength of excitation, such as the nanoparticle dimers of interest here, we argue that retardation effects alone are sufficient to explain a myriad of experimentally observed phenomenon including ODH. Though the objects have no net magnetization, the generation of helical surface currents (due to simultaneous excitation of electric and magnetic dipoles) allows for the generation of magnetic fields and responses.

To verify that such modes are indeed sustained by the dimers, we present here a systematic, quantum mechanical treatment which, though formulated with the nanosphere dimers in mind, holds for any general uniaxial object with $l \sim \lambda$. We start with the standard light-matter action Hamiltonian, which describes the material response as a function of input field. We then substitute the subsequent interaction potential into Fermi's Golden Rule (FGR) to determine the transitions allowed under such interaction. Though such a treatment is typically employed to determine molecular scattering processes, our treatment here is particularly to the electrons that comprise the metallic plasmon. We will see that simply expanding the interaction to first order in spatial dispersion, which only holds for objects with $l \sim \lambda$, the magnetic dipole and electric quadrupolar modes are excited simultaneously to and to the same order as the zeroth-order electric dipole mode.

The general form of the light-matter interaction potential, which mediates material response, is given by (5):

$$\hat{V} = \frac{i\hbar e}{2mc}\left(\vec{\nabla} \cdot \vec{A} + \vec{A} \cdot \vec{\nabla}\right) + \frac{e^2}{2mc^2}\left(\vec{A} \cdot \vec{A}\right). \tag{4.1}$$

Here, $\vec{A}$ is the vector potential, $\vec{\nabla}\cdot$ is the divergence, and $\hbar$ is reduced Planck's constant, $c$ is the speed of light, and $e$ and $m$ are the electron charge and mass, respectively. Taking only the inelastic scattering term (ignoring $\vec{A}\cdot\vec{A}$, which is just Rayleigh) and recognizing that $\vec{\nabla}\cdot\vec{A}+\vec{A}\cdot\vec{\nabla}= 2\vec{A}\cdot\vec{\nabla}$ yields instead

$$\hat{V} = \frac{i\hbar e}{mc}\vec{A}\cdot\vec{\nabla}. \tag{4.2}$$

If we assume oscillatory vector potential $\vec{A} = A_0 e^{i(\vec{k}\cdot\vec{r}-\omega t)}$ and substitute this into FGR, we find that the following transitions are allowed (*i.e.*, excitable) between initial and final states *n, m*:

$$\langle m|V(t)|n\rangle = \frac{i\hbar e}{mc}\left\langle m\middle|A_0 e^{i(\vec{k}\cdot\vec{r}-\omega t)}\cdot\vec{\nabla}\middle|n\right\rangle = \frac{i\hbar e}{mc}A_0 e^{-i\omega t}\left\langle m\middle|e^{i\vec{k}\cdot\vec{r}}\cdot\vec{\nabla}\middle|n\right\rangle. \tag{4.3}$$

For simplicity, assume that the incident field propagation is along $\hat{z}$ ($\vec{k} = k_z\hat{z}$) and the polarization is in $\hat{x}$ $\left(\vec{\nabla}= \frac{\partial}{\partial x}\right)$. Due to size considerations $(2\pi r/\lambda \sim 1)$ we expand the vector potential to first order in spatial dispersion: $e^{ikz} \approx 1 + ikz$ so that Eq. (4.3) becomes

$$\langle V\rangle = \frac{i\hbar e}{mc}\left(\left\langle m\middle|\frac{\partial}{\partial x}\middle|n\right\rangle + \left\langle m\middle|ik_z z\frac{\partial}{\partial x}\middle|n\right\rangle\right). \tag{4.4}$$

Working first with the zeroth order term (first term in parenthesis in Eq. (4.4)) – this is just the electric dipole term; the spatial derivative can be transformed here by utilizing the commutator between the Hamiltonian and position operator, recognizing that $\left[\hat{H},\hat{x}\right] = -\frac{i\hbar}{m}p_x = -\frac{\hbar^2}{m}\frac{\partial}{\partial x}$ (where $p_x$ is the linear momentum along x) so that

$$\left\langle m\middle|\frac{\partial}{\partial x}\middle|n\right\rangle = -\frac{m}{\hbar^2}\langle m|Hx - xH|n\rangle = -\frac{m}{\hbar^2}\langle m|E_m x - xE_n|n\rangle = -\frac{m\omega_{mn}}{\hbar}\langle m|x|n\rangle. \tag{4.5}$$

Now, working with the second term in the parenthesis of Eq. (4.4), let's start by adding zero in the form of $x\frac{\partial}{\partial x}$:

$$\left\langle m\left|z\frac{\partial}{\partial x}\right|n\right\rangle = \frac{1}{2}\left\langle m\left|z\frac{\partial}{\partial x} - x\frac{\partial}{\partial z}\right|n\right\rangle + \frac{1}{2}\left\langle m\left|z\frac{\partial}{\partial x} + x\frac{\partial}{\partial z}\right|n\right\rangle. \quad (4.6)$$

These terms correspond to the magnetic dipole and electric quadrupole, respectively. To see this more clearly, working first with the magnetic dipole term we substitute in $p_j = -i\hbar\frac{\partial}{\partial j}$:

$$\left\langle m\left|z\frac{\partial}{\partial x} - x\frac{\partial}{\partial z}\right|n\right\rangle = -\frac{1}{i\hbar}\left\langle m\left|z\left(-i\hbar\frac{\partial}{\partial x}\right) - z\left(-i\hbar\frac{\partial}{\partial z}\right)\right|n\right\rangle = -\frac{1}{i\hbar}\langle m|zp_x - xp_z|n\rangle$$

$$= -\frac{1}{i\hbar}\left\langle m\left|\hat{L}_y\right|n\right\rangle \quad (4.7)$$

where we have replaced $zp_x - xp_z$ with its quantum mechanical definition, orbital angular momentum operator $\hat{L}_y$. For the quadrupolar term (second term in 4.6), we once again utilize the commutator $\left[\widehat{H}, \hat{j}\right]$:

$$\left\langle m\left|z\frac{\partial}{\partial x} + x\frac{\partial}{\partial z}\right|n\right\rangle = -\frac{m}{\hbar^2}\langle m|Hxz - zxH|n\rangle = -\frac{m\omega_{mn}}{\hbar}\langle m|xz|n\rangle. \quad (4.8)$$

Combining now all three multipolar terms (final terms in Eqs. (4.5), (4.6), and (4.7)), Eq. (4.4) becomes

$$\langle V\rangle = \frac{A_0}{c}e^{-i\omega t}\left(-ie\omega_{mn}\langle m|x|n\rangle - \frac{ik_z e}{2m}\left\langle m\left|\hat{L}_y\right|n\right\rangle + \frac{k_z\omega_{mn}}{2}\langle m|xz|n\rangle\right). \quad (4.9)$$

Noting that, for the magnetic dipole $\mu_m = \frac{eL}{2m}$ and for the electric terms $\mu_e = ex$ and $q = exz$, Eq. (4.9) can be written

$$\langle V\rangle = \frac{A_0}{c}e^{-i\omega t}(-i\omega_{mn}\langle m|\mu_e|n\rangle - ik_z\langle m|\mu_m|n\rangle + \frac{k_z\omega_{mn}}{2}\langle m|q_{xz}|n\rangle. \quad (4.10)$$

Recall the quantum mechanical definition for the orbital angular momentum operator is inherently complex as it contains a linear momentum term ($\hat{L} = \vec{r} \times \vec{p}$). Forcing this term to be real by extracting the $i$ yields finally:

$$\langle V\rangle = \frac{A_0}{c}e^{-i\omega t}(-i\omega_{mn}\langle m|\mu_e|n\rangle + k_z\langle m|\mu_m|n\rangle + \frac{k_z\omega_{mn}}{2}\langle m|q_{xz}|n\rangle. \quad (4.11)$$

The derivation of (4.11) in three dimensions (propagation in $\hat{z}$ and polarization in $\hat{x}, \hat{y}$) in shown explicitly in (5). Here, the polarization is generalized into the vector $\hat{\varepsilon}$ and the transition elements into corresponding vectors ($\vec{d}_{mn}, \vec{m}_{mn}$) and dyadic ($\bar{\bar{q}}_{mn}$); all prefactors remain the same. The final result gives

$$\langle V \rangle = \frac{A_0}{c} e^{-i\omega t} \left( -i\omega_{mn} \hat{\varepsilon} \cdot \vec{d} + \vec{k} \times \hat{\varepsilon} \cdot \vec{m} + \frac{\omega_{mn}}{2} \hat{\varepsilon} \cdot \bar{\bar{q}} \cdot \vec{k} \right). \tag{4.12}$$

The quadrupolar dyadic in three dimensions is $q_{xz}\hat{x} - q_{yz}\hat{y} = \frac{\vec{q}}{2}$. Given wavevector $\vec{k} = |k|\hat{k}$ and multipoles $\vec{\alpha} = |\alpha|\hat{\alpha}$, Eq. (4.12) can be transformed into

$$\begin{aligned} \langle V \rangle &= \frac{A_0}{c} e^{-i\omega t} \left( -i\hat{\varepsilon} \cdot |d|\hat{d} + \frac{1}{\omega_{mn}} |k|\hat{k} \times \hat{\varepsilon} \cdot |m|\hat{m} + \hat{\varepsilon} \cdot |q|\hat{q} \cdot |k|\hat{k} \right) \\ &= \vec{A}' |d| \left( -i\hat{\varepsilon} \cdot \hat{d} + \frac{|k|}{\omega_{mn}} \frac{|m|}{|d|} \hat{k} \times \hat{\varepsilon} \cdot \hat{m} + |k| \frac{|q|}{|d|} \hat{\varepsilon} \cdot \hat{q} \cdot \hat{k} \right) \\ &= \vec{A}'' |d| \left( \hat{\varepsilon} \cdot \hat{d} + i\zeta_m \hat{k} \times \hat{\varepsilon} \cdot \hat{m} + i\zeta_q \hat{\varepsilon} \cdot \hat{q} \cdot \hat{k} \right) \end{aligned} \tag{4.13}$$

so that

$$\langle V \rangle \sim |d| \left( \hat{\varepsilon} \cdot \hat{d} + i\left( \zeta_m \hat{k} \times \hat{\varepsilon} \cdot \hat{m} + \zeta_q \hat{\varepsilon} \cdot \hat{q} \cdot \hat{k} \right) \right) \tag{4.14}$$

where $\zeta_m$ and $\zeta_q$ scale $m$ and $q$ relative to $d$. Equation (4.14) represents the potential between the incident light and the matter with which it interacts. Our goal in the proceeding section will be to use this interaction potential to build a matrix to describe the scattering nature of our sample, in order to determine the origins of the elusive ODH.

4.2. Construction of the sample scattering matrix

As indicated in Eq. (4.14), electromagnetic cross-coupling is induced in the medium (*e.g.*, $\hat{k} \times \hat{\varepsilon} \cdot \hat{m}$) which necessitates consideration of both the electric and magnetic field components. Since the measurements are made in the far field, the electric and magnetic fields are strictly transverse and therefore fully characterized by 2D spinors; assuming again propagation along $\hat{z}$ and polarization in $\hat{x}, \hat{y}$, the electric and magnetic field components are described as follows (12).

$$\hat{\varepsilon} = \begin{pmatrix} \varepsilon_x \\ \varepsilon_y \end{pmatrix} \tag{4.15a}$$

$$\hat{h} = \hat{k} \times \hat{\varepsilon} = \begin{pmatrix} -\varepsilon_y \\ \varepsilon_x \end{pmatrix} \tag{4.15b}$$

Our sample will be described by a 2x2 transformation matrix which acts on these 2x1 input fields. The elements of the sample interaction matrix can be directly read from Eq. (4.14). Briefly,

$$\hat{k} \times \hat{\varepsilon} = -k_z \varepsilon_y + k_z \varepsilon_x = h_x + h_y \tag{4.16a}$$

$$\hat{r} \times \hat{p} = \begin{vmatrix} \hat{x} & \hat{y} & \hat{z} \\ 0 & 0 & z \\ p_x & p_y & p_z \end{vmatrix} = -z p_y + z p_x = m_x + m_y. \tag{4.16b}$$

In a uniaxial system such as the nanosphere dimers, the multipolar moments are expected to lie along the quantization (inter-particle) axis, to the extent that a dimer oriented along the laboratory x-axis will have $\alpha_x \gg \alpha_y \to 0$. For a dimer oriented along $\hat{x}$, Eq. (4.14) becomes

$$V_x = \varepsilon_x d_x + i\zeta \left( \left(-k_z \varepsilon_y\right)\left(-z p_y\right) + \varepsilon_x q_{xz} \right) = \varepsilon_x (d_x + i q_x) + i m_x h_x. \tag{4.17}$$

In matrix form, the operator acting on the field is cast as follows:

$$\hat{V}_x = \begin{pmatrix} d_x + i q_x & i m_x \\ 0 & 0 \end{pmatrix} \begin{pmatrix} \varepsilon_x \\ h_x \end{pmatrix} = \begin{pmatrix} d_x + i q_x & i m_x \\ 0 & 0 \end{pmatrix} \begin{pmatrix} \varepsilon_x \\ \varepsilon_y \end{pmatrix} \tag{4.18}$$

using $h_x = -\varepsilon_y$. Similarly, for a y-oriented particle,

$$V_y = \varepsilon_y d_y + i\zeta\left((-k_z\varepsilon_x)(-zp_x) + \varepsilon_y q_{yz}\right) = \varepsilon_y\left(d_y + iq_y\right) + im_y h_y, \quad (4.19)$$

With corresponding matrix form

$$\hat{V}_y = \begin{pmatrix} d_y + iq_y & im_y \\ 0 & 0 \end{pmatrix}\begin{pmatrix} \varepsilon_y \\ h_y \end{pmatrix}. \quad (4.20)$$

The basis vector of Eq. (4.20) is rotated and of opposite handedness from that of Eq. (4.18). To put $V_y$ into the same basis as $V_x$, note that for a general handed vector $(1 \quad i)^T$, the rotation into the opposite handed form is achieved by

$$\begin{pmatrix} 1 \\ i \end{pmatrix} = i\begin{pmatrix} -i \\ 1 \end{pmatrix} = i\begin{pmatrix} i \\ 1 \end{pmatrix}^* \quad (4.21)$$

which, ignoring the overall phase, corresponds to a conjugate transpose. When applied to Eq. (4.20), this yields

$$\hat{V}_y = \begin{pmatrix} 0 & 0 \\ -im_y & d_y - iq_y \end{pmatrix}\begin{pmatrix} \varepsilon_x \\ \varepsilon_y \end{pmatrix}. \quad (4.22)$$

The general scattering matrix as a function of dimer orientation $\varphi$, given here by $\hat{O}_\varphi$, is then

$$\hat{O}_\varphi = \begin{pmatrix} (d_x + iq_x)\cos\varphi & im_x\cos\varphi \\ -im_y\sin\varphi & (d_y - iq_y)\sin\varphi \end{pmatrix}. \quad (4.23)$$

For a uniaxial object, Eq. (4.23) is a matrix of projections, whereby the multipolar modes are projected onto the particle long axis oriented at $\varphi$:

$$\hat{O}_\varphi = \begin{pmatrix} (d + iq)\cos\varphi & im\cos\varphi \\ -im\sin\varphi & (d - iq)\sin\varphi \end{pmatrix}. \quad (4.24)$$

The corresponding excitation probability is found by taking the product of $V$ with is Hermitian conjugate. Although the Raman process is second order in the interaction, $|V^\dagger V|^2$, the relevant physics is all contained within the first order excitation probability

$V^{\dagger}V = \langle \varepsilon_{sc} | \hat{O}_{\varphi}^{\dagger} \hat{O}_{\varphi} | \varepsilon_{in} \rangle$ and, as such, it is a suitable quantity for this analysis (13). Here, the sample scattering probability matrix is defined as

$$\hat{O}_{\varphi}^{\dagger} \hat{O}_{\varphi} = \Sigma_{\varphi} =$$

$$\begin{pmatrix} (d^2 + q^2)\cos\varphi^2 + m^2 \sin\varphi^2 & (mq + imd)\cos\varphi^2 + (mq - imd)\sin\varphi^2 \\ (mq - imd)\cos\varphi^2 + (mq + imd)\sin\varphi^2 & m^2 \cos\varphi^2 + (d^2 + q^2)\sin\varphi^2 \end{pmatrix}. \tag{4.25}$$

We recognize here the full sample scattering probability $\Sigma_{\varphi}$ as the general material polarizability tensor, $\alpha$. For a particle oriented along the x-direction ($\varphi = 0°$), the matrix has the form

$$\Sigma_x = \begin{pmatrix} d^2 + q^2 & mq + imd \\ mq - imd & m^2 \end{pmatrix} \tag{4.26}$$

while a particle oriented along the y-direction is described by

$$\Sigma_y = \begin{pmatrix} m^2 & -mq - imd \\ -mq + imd & d^2 + q^2 \end{pmatrix}. \tag{4.27}$$

The pure polarization states of $V^{\dagger}V = \langle \varepsilon_{sc} | \hat{O}_{\varphi}^{\dagger} \hat{O}_{\varphi} | \varepsilon_{in} \rangle$ can be cast into the equivalent density form, whose expectation value is given by

$$V^{\dagger}V = Tr\left(\Sigma_{\varphi} \, |\varepsilon\rangle\langle\varepsilon| \, \right). \tag{4.28}$$

The field density

$$|\varepsilon\rangle\langle\varepsilon| = \begin{pmatrix} \varepsilon_x \varepsilon_x^* & \varepsilon_x \varepsilon_y^* \\ \varepsilon_y \varepsilon_x^* & \varepsilon_y \varepsilon_y^* \end{pmatrix} \tag{4.29}$$

and sample scattering matrix $\Sigma_{\varphi}$ in this form are members of the **SU(2)** vector space. The space is completely spanned by the Pauli optical matrices:

$$\sigma_0 = \begin{pmatrix} 1 & 0 \\ 0 & 1 \end{pmatrix}, \;\; \sigma_1 = \begin{pmatrix} 1 & 0 \\ 0 & -1 \end{pmatrix}, \sigma_2 = \begin{pmatrix} 0 & 1 \\ 1 & 0 \end{pmatrix}, \sigma_3 = \begin{pmatrix} 0 & -i \\ i & 0 \end{pmatrix}, \tag{4.30}$$

which are sometimes condensed into the single vector $\vec{\sigma} = (\sigma_0 \quad \sigma_1 \quad \sigma_2 \quad \sigma_3)^T$. The field and scattering densities are subsequently decomposed into the Pauli matrices as

$$|\varepsilon\rangle\langle\varepsilon| = \vec{S} \cdot \vec{\sigma} = \sum_{i=0}^{3} S_i \sigma_i \tag{4.31a}$$

$$\Sigma_\varphi = \vec{s} \cdot \vec{\sigma} = \sum_{i=0}^{3} s_i \sigma_i \tag{4.31b}$$

where $\vec{S}$ and $\vec{s}$ are the vectors of the coefficients that weight the corresponding Pauli matrices. Any matrix $J$ in **SU(2)** is therefore describable by:

$$J = \begin{pmatrix} s_0 + s_1 & s_2 - is_3 \\ s_2 + is_3 & s_0 - s_1 \end{pmatrix}. \tag{4.32}$$

In the vector calculus of polarization specifically, these transformation in **SU(2)** proceed within the formalism of Jones calculus. Here, complex 2x2 Jones matrices describe how an optical element transforms light, which is given by a 2x1 complex vector. The strength of this formalism lies in its direct formulation from the Maxwell equations, which retains information about the relative phases of field components and material response (7). In analogy with the quantum mechanics of two-level systems, Jones vectors are confined to describing fully polarized states in the same way that wavefunctions describe pure states.

In its given form, Eq. (4.31) of the standard Jones matrix is readily compared with the sample scattering matrix, $\Sigma_\varphi$. For a particle oriented along the x-direction ($\Sigma_x$), the coefficients that weight the Pauli matrices are as follows.

$$s_0 = \frac{d^2+q^2+m^2}{2} = N \tag{4.33a}$$

$$s_1 = \frac{d^2+q^2-m^2}{2} = N' \tag{4.33b}$$

$$s_2 = mq \tag{4.33c}$$

$$s_3 = -md \tag{4.33d}$$

These coefficients are known as the Stokes parameters. Transformations can be carried out directly with their Stokes vector equivalents ($\vec{S}$ and $\vec{s}$) in the Mueller calculus formalism. Here, linear transformations are represented by scalings and rotations of the 4-element Stokes vectors in **O(3)**. Rather than the complex field vectors of Jones, Mueller calculus deals strictly with light intensities, with the general vector form (7)

$$\vec{S} = \begin{pmatrix} I_x + I_y \\ I_x - I_y \\ I_{45^\circ} - I_{-45^\circ} \\ I_{RCP} - I_{LCP} \end{pmatrix} \tag{4.34}$$

where $I_j$ is the intensity of *j*-polarized light. With this in hand, we write Eq. (4.28) as

$$V^\dagger V = \langle s|S\rangle, \tag{4.35}$$

whose true utility is realized when the interaction is visualized on the Poincare sphere. Recall that the three orthogonal axes of the sphere are defined by the Pauli matrices $\{\sigma_1, \sigma_2, \sigma_3\} = \{\sigma_z, \sigma_x, \sigma_y\}$ of spin notation, with $\sigma_0$ setting the size of the sphere as unity. The Stokes parameters $\{s_1, s_2, s_3\}$ give the projections of a vector onto each axis of the sphere, which again correspond to $x/y$, $+45°/-45°$, $RCP/LCP$, respectively. In this way, both the field and scattering vector can be directly cast onto the sphere; take, for example, the scattering matrix $\Sigma_x$ given by Eq. (4.26). Using the definitions of $\{s_i\}$ given in Eq. (4.33),

$$\vec{s}_x = \begin{pmatrix} s_1 \\ s_2 \\ s_3 \end{pmatrix} = \frac{1}{N}\begin{pmatrix} (d^2 + q^2 - m^2)/2 \\ mq \\ -md \end{pmatrix} \tag{4.36}$$

where $s_0 = N = (d^2 + q^2 + m^2)/2$ normalizes the vector to unity. This vector is illustrated in Fig.7 for $\{d = m = q = 1\}$. More generally, though, the physical meaning of the dimer Stokes parameters are elucidated from Eq. (4.33). Parameter $s_1$ defines the

extent of the uniaxial nature of the dimer (*e.g.*, differential long versus short axis scattering response). Parameter $s_2$ is the $\pm 45°$ scattering linear dichroism, and $s_3$ is the scattering circular dichroism (*i.e.*, optical activity). In accordance with its historical definition, we see that the chirality is determined by the product of an electric and magnetic dipole. Positive values of $s_3$ direct the Stokes sample vector toward the north pole of the sphere, and correspond to right-handed scatterers. Conversely, overall negative $s_3$ gives rise to left-handed objects.

As discussed in Chapter 2, the light vector for the continuous QW rotation experiment, defined here as $\vec{S}_{qw}$, traces out a figure-eight on the surface of the Poincare sphere. Using the definitions for the optical elements that are standard within Mueller, we can express the functional form of the light path as follows.

$$\vec{S}_{qw} = R_\chi^T \cdot QW_v \cdot R_\chi \cdot \vec{S}_v = \begin{pmatrix} -\cos(2\chi)^2 \\ \cos(2\chi)\sin(2\chi) \\ -\sin(2\chi) \end{pmatrix} \tag{4.37}$$

Here, $R_\chi$ is the **O(3)** rotation matrix, $QW_v$ the QW originally vertically-oriented, and $S_v$ is the incident vertical light. The resulting interaction of Eq. (4.37) with the sample Stokes vector, $\langle s|S\rangle = \vec{s} \cdot \vec{S}_{qw}$, projects the incident light vector onto the sample scattering vector. Geometrically, this corresponds simply to a scaling of $\vec{s}$ – its direction does not change, though its magnitude is mediated by $\vec{S}_{qw}$ as a function of QW orientation $\chi$. In the example given in Fig. 7 for $\vec{s}_x$, $\vec{s}_x \cdot \vec{S}_{qw}$ is maximum when the incident light is of the same handedness of the sample (here, LCP), and minimum when it is opposed. Note that it is the inclusion of the linear dichroism term, $mq$, which dictates the survival of this

interaction. For the case $d = m = 1, q = 0$, the vector $\vec{s}_x(q = 0) = (0, 0, -1)^T$ points directly at the south pole so that when light is perfectly RCP, $\vec{s}_x(q = 0) \cdot \vec{S}_{RCP} = 0$.

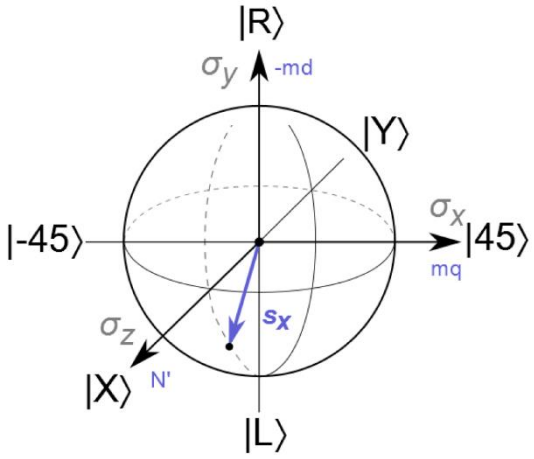


Figure 4.1: Stokes vectors and the Poincare sphere. Representation of an example sample scattering vector $\vec{s}_x$ on the Poincare sphere. Sphere axes are defined by the Pauli spin matrices with corresponding polarization states as indicated by the given kets. The projections of the vector onto each axis are determined by the Stokes parameters, the forms of which are given in purple.

## 4.3. Origins of ODH

The observed intensity patterns from continuous QW rotations, such as the one presented in Fig.6 for dimer 5, can be fit to the following equation to extract the Stokes parameters $s_i$

$$I(\chi) = \vec{s}_x \cdot \vec{S}_{qw} = s_0 - s_1 \cos(2\chi)^2 + s_2 \cos(2\chi) \sin(2\chi) - s_3 \sin(2\chi) \quad (4.38)$$

which are then used to build the sample Jones scattering matrix:

$$J = \Sigma_\varphi = \begin{pmatrix} s_0 + s_1 & s_2 - is_3 \\ s_2 + is_3 & s_0 - s_1 \end{pmatrix}. \quad (4.39)$$

Fits to the original ($\varphi = 0°$) and rotated ($\varphi = 90°$) orientation of dimer 5 yield Stokes vectors

$$\vec{s}_x(\varphi = 0°) = \begin{pmatrix} 1 \\ 0.5 \\ 0.5 \\ 0.5 \end{pmatrix}, \ \vec{s}_y(\varphi = 90°) = \begin{pmatrix} 1 \\ 0.5 \\ 0.5 \\ 0.5 \end{pmatrix} \quad (4.40)$$

with associated scattering matrices

$$J_x = \Sigma_x = \begin{pmatrix} 1.5 & 0.5 - 0.5i \\ 0.5 + 0.5i & 0.5 \end{pmatrix}, \; J_y = \Sigma_y = \begin{pmatrix} 0.5 & -0.5 + 0.5i \\ -0.5 - 0.5i & 1.5 \end{pmatrix} \quad (4.41)$$

These matrices reproduce the observed response very well (Fig. 8a, 8c). One would expect the effects of rotating the sample 90° in-plane to be given by a 90° rotation of the scattering matrix, such that

$$\Sigma_y = R^T(90°) \cdot \Sigma_x \cdot R(90°) = \begin{pmatrix} 0.5 & -0.5 - 0.5i \\ -0.5 + 0.5i & 1.5 \end{pmatrix} \quad (4.42)$$

where $R(\varphi)$ is the standard Euclidean rotation matrix

$$R(\varphi) = \begin{pmatrix} \cos\varphi & \sin\varphi \\ -\sin\varphi & \cos\varphi \end{pmatrix}. \quad (4.43)$$

This, of course, should not result in a change in handedness – indeed, the response predicted by a simple solid body rotation of the matrix $\Sigma_x$ is shown in Fig. 8b. Comparison of the requisite scattering matrices given in Eq. (4.41) reveal what has already been implied in Section 4.2: in order for the handedness to invert upon sample rotation, the sign of the complex parameter $s_3$ must change upon rotation.

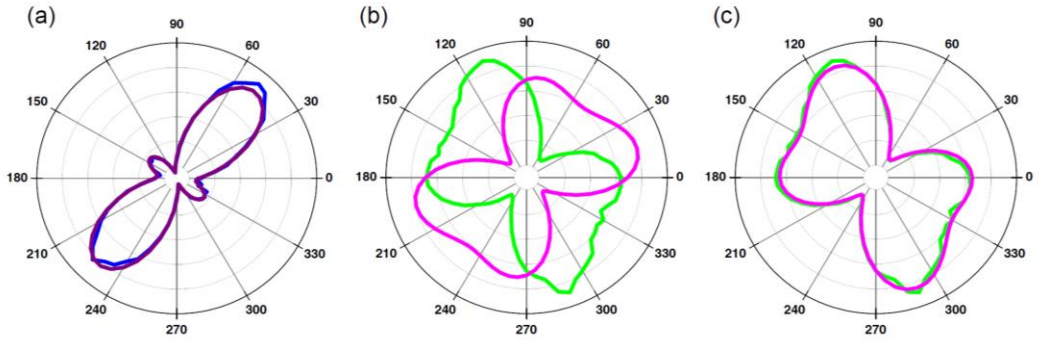


Figure 4.2: Actual and predicted effects of sample orientation. (a) Response of dimer 5 at its original position $\varphi = 0°$ (blue), overlaid with its reproduction using $\Sigma_x$ (purple). (b) Predicted response of dimer 5 after its original position matrix, $\Sigma_x$, is subject to a 90° solid-body in-plane rotation (pink), overlaid with its actual response (green). (c) Response of dimer 5 at its rotated position $\varphi = 90°$ (green), overlaid with its reproduction using $\Sigma_y$ (pink).

The only mechanism by which such a transformation is achievable is an additional *complex conjugation* upon rotation. This complex conjugation is immediately indicative of a particular type of symmetry – namely, that of time reversal. In order for a particle to remain invariant upon the coordinate transformation, it appears that time must simultaneously be inverted (14). This signals that the response is PT (parity-time) invariant, which can be understood by the following considerations. Here for simplicity we will work with the minimal system which reproduces the effect: an electric and magnetic dipole, represented here by a polar and axial vector, respectively. This pair is easily seen to be PT invariant if we recognize that parallel $d$ and $m$ describe a right helix $\psi(R)$ while antiparallel $d$ and $m$ describe a left helix $\psi(L)$. Under the parity operator $\hat{P}$, $d$ is odd and $m$ is even, such that $\hat{P}\big(\psi(R)\big) = \psi(L)$ (Fig. 9). Under time reversal, it is now $d$ is even and $m$ odd; similarly, $\hat{T}\big(\psi(R)\big) = \psi(L)$. Under joint PT, this results in $\hat{T}\left(\hat{P}\big(\psi(R)\big)\right) = -\psi(R)$. In this way, the complex conjugation is identified as the time reversal under the rotation, necessary to conserve the PT invariance of the dimer.

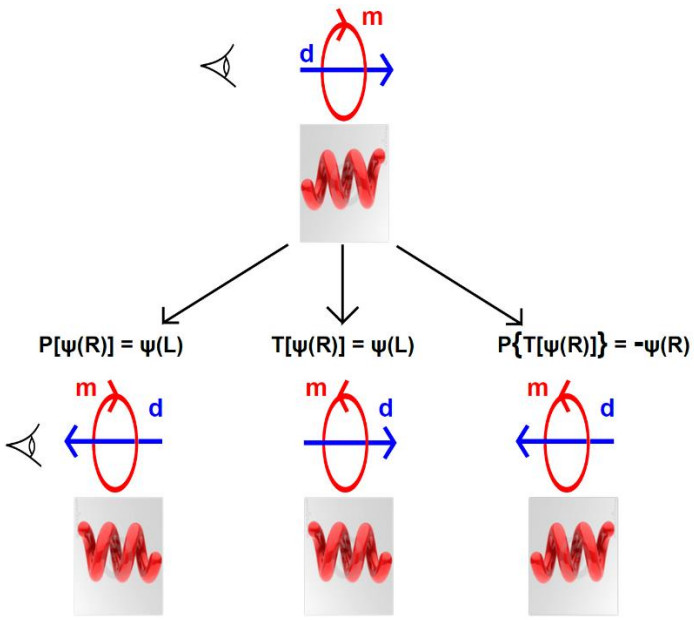


Figure 4.3: The effects of the parity and time reversal operators, here on a system consisting of an electric and magnetic dipole. A stationary observer sees a RH helix from the combined effect of an electric dipole along $\hat{x}$ and a clockwise-circulating magnetic dipole. Under $\hat{P}$, the electric dipole is now along $-\hat{x}$ while the magnetic dipole maintains its original clockwise circulation. From the same observation point, this construction now gives rise to a LH helix. The time reversal case is treated similarly, noting now that the electric dipole remains along $\hat{x}$ while the sense of rotation of the magnetic dipole changes to counter-clockwise. The combined effect of a PT operation, then, is to leave the original handedness unchanged.

## 4.4. Physical Equivalence

Using the preceding geometric considerations of $\vec{s} \cdot \vec{S}$ and the form of the sample scattering matrix given in Eq. (4.25),

$$\hat{O}_{\varphi}^{\dagger}\hat{O}_{\varphi} = \Sigma_{\varphi} =$$

$$\begin{pmatrix} (d^2+q^2)\cos\varphi^2 + m^2\sin\varphi^2 & (mq+imd)\cos\varphi^2 + (mq-imd)\sin\varphi^2 \\ (mq-imd)\cos\varphi^2 + (mq+imd)\sin\varphi^2 & m^2\cos\varphi^2 + (d^2+q^2)\sin\varphi^2 \end{pmatrix},$$

(4.25)

we can also generate a physical equivalence for our uniaxial scatterer. For simplicity, we will first work with the minimal system which reproduces the ODH ($q = 0$). The excitation probability is then reduced to

$$\Sigma_\varphi = \begin{pmatrix} d^2\cos\varphi^2 + m^2\sin\varphi^2 & imd\cos\varphi^2 - imd\sin\varphi^2 \\ -imd\cos\varphi^2 + imd\sin\varphi^2 & m^2\cos\varphi^2 + d^2\sin\varphi^2 \end{pmatrix}. \quad (4.44)$$

For the sake of transparency, and without loss of generality, we set $d = m = 1$ and decompose Eq. (4.44) into its orthogonal components:

$$\Sigma_\varphi = \begin{pmatrix} 1 & i \\ -i & 1 \end{pmatrix}\cos\varphi^2 + \begin{pmatrix} 1 & -i \\ i & 1 \end{pmatrix}\sin\varphi^2. \quad (4.45)$$

The matrices given in Eq. (4.45) are nothing more than the right and left circular polarization projectors,

$$\Sigma_\varphi = |R\rangle\langle R|\cos\varphi^2 + |L\rangle\langle L|\sin\varphi^2, \quad (4.46)$$

so that the sample acts as a superposition of left and right circular polarizers, weighted by the sample orientation $\varphi$. At $\varphi = 0°$, for example, the response is that of a pure right circular polarizer that passes RCP and fully reject LCP. The converse is true for $\varphi = 90°$, at which the sample acts as a left circular polarizer. At intermediate orientations, the relative strengths of the right and left projectors are given by $\cos\varphi^2$ and $\sin\varphi^2$, respectively.

Reinserting the full, general response $\{d, m, q\}$, we have

$$\Sigma_\varphi = \begin{pmatrix} d^2 + q^2 & mq + imd \\ mq - imd & m^2 \end{pmatrix}\cos\varphi^2 + \begin{pmatrix} m^2 & -mq - imd \\ -mq + imd & d^2 + q^2 \end{pmatrix}\sin\varphi^2. \quad (4.47)$$

Eq. (4.47) is a superposition of two elliptical polarization projectors of opposite handedness ($md$) and direction of tilt ($q/m$). This is a striking result, as it is the optical equivalent of a quantum mechanical superposition state, here made all the more unique as it implies two simultaneous measurements carried out on a single photon.

Reinserting the full, general response of $\{d, m, q\}$ active, we have

$$\Sigma_\varphi = \begin{pmatrix} d^2+q^2 & mq+imd \\ mq-imd & m^2 \end{pmatrix} \cos\varphi^2 + \begin{pmatrix} m^2 & -mq-imd \\ -mq+imd & d^2+q^2 \end{pmatrix} \sin\varphi^2. \quad (4.48)$$

Working first with $\Sigma_x$ (first term of Eq. (4.48)), we find that the matrix has the following Eigenvalues and vectors:

$$\lambda_{x,1} = 0,\ \vec{v}_{x,1} = \begin{pmatrix} 1 \\ -\frac{d+iq}{im} \end{pmatrix} \quad (4.49a)$$

$$\lambda_{x,2} = 1,\ \vec{v}_{x,2} = \begin{pmatrix} 1 \\ \frac{m}{q+id} \end{pmatrix} \quad (4.49b)$$

which reveals the basis vectors of $\Sigma_x$ are elliptical polarizations. To see this more clearly, working with the non-trivial Eigenvector $\vec{v}_{x,2}$:

$$\vec{v}_{x,2} = \begin{pmatrix} 1 \\ \frac{m}{q+id} \end{pmatrix} = \begin{pmatrix} 1 \\ \frac{mq}{d^2+q^2} - i\frac{md}{d^2+q^2} \end{pmatrix} = \begin{pmatrix} 1 \\ b-ic \end{pmatrix}. \quad (4.50)$$

In general, any elliptical polarization vector is described by

$$E_{ell} = \begin{pmatrix} A \\ B \pm iC \end{pmatrix} \quad (4.51)$$

Where $A$ and $C$ give the horizontal and vertical components, respectively, of the ellipse, and $B$ defines its tilt. The $\pm$ dictates the sense of rotation, with the convention $+ \rightarrow LCP$ and $- \rightarrow RCP$. Equation (4.50), then, describes a RH ellipse with major axis $A = 1$, minor axis $C = md/(d^2+q^2)$, and tilt $B = mq/(d^2+q^2)$. Conversely, the same manipulation of $\Sigma_y$ yields an identical solution set, with swapped non-trivial Eigenvectors

$$\lambda_{y,1} = 0,\ \vec{v}_{y,1} = \begin{pmatrix} 1 \\ \frac{m}{q+id} \end{pmatrix} \quad (4.52a)$$

$$\lambda_{y,2} = 1,\ \vec{v}_{y,2} = \begin{pmatrix} 1 \\ -\frac{d+iq}{im} \end{pmatrix} \quad (4.52b)$$

identifying it as a LH elliptical projector with $A = 1$, $C = d/m$, and tilt $B = -q/m$.

# 5. IMPLICATIONS

## 5.1. Wave propagation in bi-isotropic media

We can now extend the previous treatment to direct comparison with well-known material parameters. As previously discussed, it is evident that the system generates significant electromagnetic cross-coupling in both linear ($mq$) and circular ($md$) bases. A material consisting of such uniaxial scatterers will then be, in the most general case, bi-isotropic (BI). For a general BI medium, cross coupling between the electric and magnetic field components within the medium is described by the well-known constitutive equations (15)

$$\vec{B} = \mu\vec{H} + (\chi + i\kappa)\vec{E}. \tag{5.1a}$$

$$\vec{D} = \epsilon\vec{E} + (\chi - i\kappa)\vec{H} \tag{5.1b}$$

Here, $\vec{D}$ and $\vec{B}$ are the electric displacement and magnetic inductance fields generated in the medium, and $\vec{E}$ and $\vec{H}$ are the exciting external electric and magnetic fields. Parameters $\chi$ and $\kappa$ are describe, respectively, the non-reciprocity and chirality of the material. These terms are what allows the application of an electric field to generate magnetic response (and vice-versa) within the medium.

BI media are birefringent and consequently, the refractive index of light in the medium depends heavily on its polarization. Here, we present a straightforward derivation of the wave propagation and resulting split index in a BI material, which assumes no underlying basis. We start with the source-free Faraday and modified Ampere's law (16)

$$\vec{\nabla} \times \vec{E} = -\frac{\partial}{\partial t}\vec{B} \tag{5.2a}$$

$$\vec{\nabla} \times \vec{H} = \frac{\partial}{\partial t}\vec{D}. \tag{5.2b}$$

Inserting Eqs. (5.1a) into (5.2a) and (5.1b) into (5.2b) gives, respectively,

$$\vec{\nabla} \times \vec{E} = -(\chi + i\kappa)\frac{\partial}{\partial t}\vec{E} - \mu\frac{\partial}{\partial t}\vec{H} \tag{5.3a}$$

$$\vec{\nabla} \times \vec{H} = (\chi - i\kappa)\frac{\partial}{\partial t}\vec{H} + \epsilon\frac{\partial}{\partial t}\vec{E}. \tag{5.3b}$$

Now, taking the curl of Eq. (5.3a) and noting that $\left[\frac{\partial}{\partial t}, \nabla \times\right] = 0$,

$$\vec{\nabla} \times \vec{\nabla} \times \vec{E} = -(\chi + i\kappa)\frac{\partial}{\partial t}\vec{\nabla} \times \vec{E} - \mu\frac{\partial}{\partial t}\vec{\nabla} \times \vec{H} \tag{5.4}$$

and substituting in Eq. (5.3b) gives

$$\vec{\nabla} \times \vec{\nabla} \times \vec{E} = -(\chi + i\kappa)\frac{\partial}{\partial t}\vec{\nabla} \times \vec{E} - \mu\epsilon\frac{\partial^2}{\partial t^2}\vec{E} - \mu(\chi - i\kappa)\frac{\partial}{\partial t}\left(\frac{\partial}{\partial t}\vec{H}\right). \tag{5.5}$$

Rearranging Eq. (5.3a) in terms of $\mu\frac{\partial}{\partial t}\vec{H}$ and inserting into Eq. (5.5) yields, finally,

$$\vec{\nabla} \times \vec{\nabla} \times \vec{E} = -(\chi + i\kappa)\frac{\partial}{\partial t}\vec{\nabla} \times \vec{E} - \mu\epsilon\frac{\partial^2}{\partial t^2}\vec{E} - (\chi - i\kappa)\frac{\partial}{\partial t}\left(-(\chi + i\kappa)\frac{\partial}{\partial t}\vec{E} - \vec{\nabla} \times \vec{E}\right)$$

$$= -2i\kappa\frac{\partial}{\partial t}\vec{\nabla} \times \vec{E} + (\chi^2 + \kappa^2 - \mu\epsilon)\frac{\partial^2}{\partial t^2}\vec{E}. \tag{5.6}$$

Based on the definition of the Fourier transform, $\frac{\partial}{\partial t} = \omega$, Eq. (5.6) can be written

$$0 = \vec{\nabla} \times \vec{\nabla} \times \vec{E} + 2i\omega\kappa\vec{\nabla} \times \vec{E} - \omega^2(\chi^2 + \kappa^2 - \mu\epsilon)\frac{\partial^2}{\partial t^2}\vec{E}. \tag{5.7}$$

Eq. (5.7) describes the propagation of electromagnetic waves in the bi-isotropic medium, which is governed by the solutions

$$k_{\pm} = \omega\left(\sqrt{\mu\epsilon - \chi^2} \pm \kappa\right), \tag{5.8}$$

with corresponding refractive indices

$$n_{\pm} = \frac{k_{\pm}}{\omega} = \sqrt{\mu\epsilon - \chi^2} \pm \kappa. \tag{5.9}$$

## 5.2. Connecting material parameters with multipolar modes

In order to facilitate direct comparison of the material parameters with the known multipolar modes of the dimer antenna, Eqs. (5.1a) and (5.1b) are cast into matrix form as follows.

$$\begin{pmatrix} \vec{D} \\ \vec{B} \end{pmatrix} = \begin{pmatrix} \epsilon & \chi - i\kappa \\ \chi + i\kappa & \mu \end{pmatrix} \begin{pmatrix} \vec{E} \\ \vec{H} \end{pmatrix}. \tag{5.10}$$

Inspection alone allows us to immediately equate parameters $\{\epsilon, \mu, \chi, \kappa\}$ of the matrix presented in Eq. (5.10) with multipolar modes presented in the matrix of Eq. (4.26) for the x-oriented particle. We find that

$$\epsilon = d^2 + q^2 \tag{5.11a}$$

$$\mu = m^2 \tag{5.11b}$$

$$\chi = mq \tag{5.11c}$$

$$\kappa = -md. \tag{5.11d}$$

These definitions can then be used to recast the indices of Eq. (5.9) as

$$n_{\pm} = \sqrt{(d^2 + q^2)m^2 - (mq)^2} \mp md = \sqrt{m^2d^2 + m^2q^2 - m^2q^2} \mp md \tag{5.12}$$

which, of course, simplifies to

$$n_{\pm} = \sqrt{m^2d^2} \mp md = md \mp md \tag{5.13}$$

so that the final indices are

$$n_+ = 0 \tag{5.14a}$$

$$n_- = 2md = -2\kappa \tag{5.14b}$$

with corresponding propagation factors $k_+ = 0$ and $k_- = 2\omega md = -2\omega\kappa$. (Note that the sign convention is a little unusual here as the chirality term is negatively signed: $\kappa = -md$, based on the standard Jones convention of the sign of $s_3$.) From this, it is evident

that only one Eigenmode (here, $k_-$, usually distinguished as LCP) propagates in the medium with standard refractive index. The effect on non-reciprocity, while interesting in its own right, does not explicitly factor into the final index here – the index depends solely on the chirality of the medium, and its sign is determined by the relative signs of $m$ and $d$. This is a very interesting case of chirality only defining the refractive index for this mode, one that is distinct from chiral nihility (where $\epsilon = \mu = 0$ but $\kappa \neq 0$). In the case of chiral nihility, negative index is indeed achievable, but there are still two Eigenwaves that persist in the medium with equal but opposite propagation constants. Here, the other index is zero, indicating that a standing wave of constant phase is generated under RCP excitation.

Though the automatic generation of negative index here is interesting in its own right, the observed ODH of the dimers adds an additional layer of intrigue that is, as of yet, largely unheard of. As the handedness, determined by the relative signs of $m$ and $d$, is controlled by the in-plane orientation of the dimer, so too is the sign of the index. Such an effect generates a novel system which, by simple rotation, can be continuously varied from positive → zero → negative index for a given CPL.

### 5.3. Applications

The most immediate application for such a material is in the generation of orientation-dependent negative index films. In this case, the material would consist of stacked films, with each film containing an array of nanodimers embedded in a non-interfering matrix such as silicon nitride or sol-gel. As the junction asymmetry is what

dictates handedness at a given orientation, nanodimers could feasibly be batch fabricated to have identical morphological features, *e.g*., via photolithography.

Though such a film would only display variable negative index under CPL, it shows a much broader spectral range than previous materials. As shown in Fig. 10, gold nanodimers have a large scattering cross sections (which are necessary to generate the large SERS OA) that extend throughout the near-UV and visible range. Particularly in the range of 300-400 nm, the cross section dominates the extinction spectrum, allowing for high scattering with relatively low loss and correspondingly high figures-of-merit.

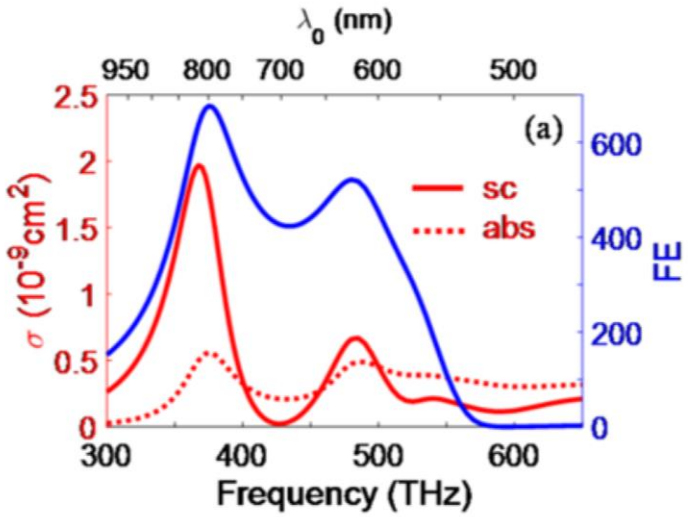


Figure 5.1: Typical dimer extinction specrum. Scattering (red solid) and absorption (red dashed) cross-section and field enhancement (blue) spectrum of a symmetric nanodimer excited with light polarized along its long axis (17).

In addition to the negative index sustained in one CPL mode of the medium, the zero-index mode is of equal interest as it has promising applications in optical circuits and quantum computing. Further studies will verify the validity of these indices, but the

preceding treatment has provided a general proof-of-concept that illustrates the utility such plasmonic nantenna have in the world of applied optoelectronics.

# 6. SUMMARY AND CONCLUSIONS

Ultimately, we have experimentally verified orientation-dependent handedness of plasmonic nanodimer antennas, where the handedness itself is a consequence of the multipolar modes the dimer sustains. There are a number of notable implications that fall out of this treatment. First, we recognize that the typical dipolar Raman response (in which all four interactions are dipole coupled to the external electric field, valid only in the long-wave limit) is now replaced with a highly nonlocal response. Expanding the light-matter potential which mediates the interaction to first order in spatial dispersion naturally leads to additional magnetic dipolar and electric quadrupolar terms. Indeed, we see that all three multipolar terms are necessary to accurately reproduce both linear and circular optical activity observed. The superposition of $\{d, m, q\}$ terms has no classical equivalent, and that all three transitions are simultaneously on resonance conveys that the system sustains angular momentum states. The relative magnitudes of the electric and magnetic dipoles $|m|^2/|d|^2 \sim 1$ are also of note – we now have a nonmagnetic sample that is capable of generating magnetic response to the same order as the electric.

Additionally, the observed symmetry breaking in the circular OA experiments provides further support for extension of the plasmonic hybridization model. In analogy with the linear combination of atomic orbitals utilized in the description of diatomic molecules, the composite dimer (molecule) may be decomposed into its two individual spheres (atoms). Each sphere, based on its size and asphericities, has its own associated plasmonic resonances, given by its angular momentum states. The

subsequent coupling of the states gives rise to split dimer energy states, much like the bonding and anti-bonding orbitals of molecular orbital theory (18).

These conclusions are all understood within the framework of the spin vector calculus of polarization, with the sample interaction matrix containing the full response of the dimer under all polarization-resolved experiments. Using the complete interaction matrix, the behavior of the antenna under a variety of experiments are accurately fit and predicted. The information uncovered in these experiments lends itself to a variety of applications, perhaps most notable the generation of broadband, controllable negative index films for the visible regime. Though this treatment was formulated with an eye toward the gold nanodimers specifically, it was presented in a general fashion that holds for any uniaxial plasmonic objects with dimensions on the order of the wavelength of excitation and has important implications for bi-isotropic media.

# REFERENCES


1. Kneipp, K.; Wang, Y.; Kneipp, H.; Perelman, L. T.; Itzkan, I.; Dasari, R. R.; Feld, M. S. Single molecule detection using surface-enhanced Raman scattering (SERS). *Physical Review Letters* **1997**, *79*, 1667-1670.
2. Sharma, B.; Frontiers, R. R.; Henry, A. I.; Ringe, E.; Van Duyne, R. P. SERS: Materials, applications, and the future. *Materials Today* **2012**, *15*, 16-25.
3. Kleinman, S. L.; Sharma, B.; Blaber, M. G.; Henry, A. I.; Valley, N.; Freeman, R. G.; Natan, M. J.; Schatz, G. C.; Van Duyne, R. P. Structure enhancement factor relationships in single gold nanoantennas by surface-enhanced Raman excitation spectroscopy. *Journal of the American Chemical Society* **2013**, *153*, 301-308.
4. Alu, A.; Egheta, N. Hertzian plasmonic nanodimer as an efficient optical nanoantenna. *Physical Review B* **2008**, *78*, 1-6.
5. Schatz, G. C.; Ratner, M. A. *Quantum Mechanics in Chemistry*, 1st ed.; Dover: New York, 2002.
6. Banik, M.; Rodriguez, K.; Apkarian, V. A. Multipolar Raman scattering on plasmonic nanoantennas. *In preparation*, **2018**.
7. Kliger, D. S.; Lewis, J. W.; Randall, C. E. *Polarized Light in Optics and Spectroscopy*, 1st ed.; Academic Press: Michigan, 1990.
8. Baron, L. D.; Hecht, L.; Blanch, E. E.; Bell, A. F. Solution structure and dynamics of biomolecules from Raman optical activity. *Progress in Biophysics and Molecular Biology* **2000**, *73*, 1-49.
9. Atkins, P. W.; Baron, L. D. Rayleigh scattering of polarized photons by molecules. *Molecular Physics* **1969**, *16*, 453-466.

10. Plum, E.; Liu, X. X.; Fedotoc, V. A.; Chen, Y.; Tsia, D. P.; Zheludev, N. I. Metamaterials: Optical activity without chirality. *Physical Review Letters* **2009**, *102*.
11. Efrati, E.; Irvine, W. T. M. Orientation-dependent handedness and chiral design. *Physical Review X* **2014**, *4*, 1-12.
12. Jackson, J. D. *Classical Electrodynamics*, 3rd ed.; John Wiley & Sons: New Jersey, 1999.
13. Mukamel, S. *Principles of nonlinear optical spectroscopy*, 1st ed.; Oxford University Press, Inc.: New York, 1995.
14. Raab, R. E.; de Lange, O. L. *Multipole Theory in Electromagnetism*, 1st ed.; Clarendon Press: Oxford, 2005.
15. Kong, J. A. *Electromagnetic Waves Theory*; EMW: Massachusetts, 2008.
16. Born, M.; Wolf, E. *Principles of Optics*, 7th ed.; Pergamon Press Ltd: Massachusetts, 2011.
17. Tork Ladani, F. *Electrodynamics of Illuminated Nanojunctions*; Faezeh Tork Ladani: California, 2017.
18. Wang, H.; Brandl, D. W.; Nordlander, P.; Halas, N. J. Plasmonic nanostructures: Artificial molecules. *Accounts in Chemical Research* **2007**, 40, 53-62.